

Development of a Multiparametric Voxel-Based Magnetic Resonance Imaging Biomarker for Early Cancer Therapeutic Response Assessment

Craig J. Galbán¹, Benjamin Lemasson¹, Benjamin A. Hoff¹, Timothy D. Johnson², Pia C. Sundgren^{1,3}, Christina Tsien⁴, Thomas L. Chenevert¹, and Brian D. Ross¹

Departments of ¹Radiology and ²Biostatistics, University of Michigan, Ann Arbor, MI; ³Faculty of Medicine, Department of Clinical Sciences/Diagnostic Radiology, Lund University, Lund, Sweden; and ⁴Department of Radiation Oncology, Washington University, St. Louis, MO

Corresponding Author:

Brian D. Ross, PhD

University of Michigan School of Medicine, Center for Molecular Imaging and Department of Radiology, 109 Zina Pitcher Place, Ann Arbor, MI; E-mail: bdross@umich.edu

Key Words: treatment response assessment, glioma, imaging biomarker, parametric response map

Abbreviations: Apparent diffusion coefficient (ADC), area under the curve (AUC), blood–brain barrier (BBB), confidence interval (CI), dynamic susceptibility contrast (DSC), diethylenetriamine pentaacetic acid (DTPA), diffusion-weighted (DW), functional diffusion mapping (fDM), field of view (FOV), gadolinium (Gd), glioblastoma (GBM), multiparametric PRM (mPRM), number of averages (NS), parametric response map (PRM), Response Assessment in Neuro-Oncology Working Group (RANO), relative cerebral blood volume (rCBV), echo time (TE), retention time (TR), receiver operating characteristic (ROC)

ABSTRACT

Quantitative magnetic resonance imaging (MRI)-based biomarkers, which capture physiological and functional tumor processes, were evaluated as imaging surrogates of early tumor response following chemoradiotherapy in glioma patients. A multiparametric extension of a voxel-based analysis, referred as the parametric response map (PRM), was applied to quantitative MRI maps to test the predictive potential of this metric for detecting response. Fifty-six subjects with newly diagnosed high-grade gliomas treated with radiation and concurrent temozolomide were enrolled in a single-site prospective institutional review board-approved MRI study. Apparent diffusion coefficient (ADC) and relative cerebral blood volume (rCBV) maps were acquired before therapy and 3 weeks after therapy was initiated. Multiparametric PRM (mPRM) was applied to both physiological MRI maps and evaluated as an imaging biomarker of patient survival. For comparison, single-biomarker PRMs were also evaluated in this study. The simultaneous analysis of ADC and rCBV by the mPRM approach was found to improve the predictive potential for patient survival over single PRM measures. With an array of quantitative imaging parameters being evaluated as biomarkers of therapeutic response, mPRM shows promise as a new methodology for consolidating physiologically distinct imaging parameters into a single interpretable and quantitative metric.

INTRODUCTION

The prognosis of glioblastoma (GBM) patients remains dismal because with the current standard of treatment patients have an average median survival of only 14 to 16 months (1, 2). Radiation therapy with concomitant temozolomide continues to be the standard of care for treatment of patients with GBM, and new therapies are urgently needed. Improving patient management (and ultimately the outcome) will require more sensitive and optimized imaging outcome metrics that will provide earlier biomarkers of therapeutic response accompanied by improved therapeutic strategies. Determining treatment response and clinical decision-making is currently based on radiologically assessing tumor volume measurements 10 weeks after the initiation of treatment. However, evaluating GBM magnetic resonance im-

aging scans (MRIs) requires differentiating responding tumors from progressive disease, which can be complicated by alterations in MRI tumor contrast as a result of therapeutically associated disruption of the blood–brain barrier (BBB), a phenomenon termed pseudoprogression that mimics true disease progression (3, 4). Thus, identifying neuroimaging methods that can assess treatment response early as well as distinguishing pseudoprogression from tumor progression would be a major advance in neuroradiology and the clinical management of GBM patients (5). Because changes in imaging tumor volume measurements can be confounded by BBB permeability changes along with inflammatory processes, efforts to improve the accuracy of patient response assessment have resulted in updated standardized clinical response criteria published by the Response Assessment in

Neuro-Oncology Working Group (RANO) (4). These new criteria address limitations with the previous response assessment criteria (Macdonald criteria) (6) by advocating the use of additional physiologically sensitive imaging biomarkers for a more accurate tumor response assessment. RANO emphasized that future response criteria will integrate newly advanced MRI techniques such as perfusion imaging (4) after rigorous clinical validation. Thus, new developments will require integrating not only 1 but multiple MRI parameters (anatomical and/or physiological) to simultaneously follow morphological and physiological modifications induced by current and emerging therapies.

Anatomical MRIs, clinical status, and corticosteroid-dependency assessment are the standards for treatment response assessment in GBM patients. Quantitative MRI may provide complementary information related to early changes in tumor pathophysiology following treatment interventions. Quantitative MRI metrics widely under evaluation as metrics of tumor response include relative cerebral blood volume (rCBV) and apparent diffusion coefficient (ADC). Tumor hemodynamics can be assessed and quantified using rCBV metrics obtained through dynamic susceptibility contrast (DSC) MRI exams (7-10). This measure, as well as other MRI-based hemodynamic parameters, has shown promise as a surrogate of clinical outcome for GBM patients treated with chemoradiotherapy as well as with anti-vascular/antiangiogenic agents (7, 8, 11-13). In addition, diffusion-weighted MRI (DW-MRI) has emerged as a method capable of measuring the random thermal (Brownian) motion of water molecules within tumor tissue and as such is sensitive to therapeutically associated changes in the tumor microenvironment (14-19). A decrease in tumor cellularity resulting from the killing of tumor cells following therapy has been associated with an increase in water diffusivity reflected in the ADC (15). This trend has been observed in preclinical and clinical studies, supporting the notion of DW-MRI as a surrogate imaging biomarker for treatment response assessment in oncology (20-22).

Evaluating the efficacy of quantitative imaging as biomarkers of therapeutic response has relied on obtaining summary statistics (eg, mean and median) over the entire tumor volume. The attractiveness of this analytical approach is the ease of implementation, reduction to a single scalar quantity, and the availability of software to implement such an analysis. Nonetheless, this approach has limitations because statistical measures calculated from quantitative tumor values can become attenuated when tumors exhibit heterogeneities in their response pattern; that is, different parts of the glioma respond differently to treatment (23, 24). To address this issue, a voxel-based method referred to as a parametric response map (PRM) has been developed that overcomes the lack of sensitivity in histogram-based techniques to quantify the evolution of treated tumors using quantitative maps (11, 25). In the context of DW-MRI, PRM is referred to as functional diffusion mapping (fDM) and has been shown to be an independent indicator of overall survival in a cohort of glioma patients (20, 25). The fDM imaging biomarker has also been demonstrated to predict outcomes in bone metastases and breast cancer (26). In 2009, PRM was demonstrated to improve the effectiveness of rCBV (11, 27) in predicting overall survival in glioma patients treated with

chemoradiotherapy. In these studies, a larger tumor portion of PRM_{rCBV} predicted shorter overall survival. More importantly, PRM was described as a general analytical technique that could be applied to multimodal quantitative maps for voxel-based tracking of disease status (11) and progression and has since been applied across a wide variety of imaging parameters (28-30).

This study reports the outcome of a prospective single-center trial of glioma patients that evaluated the ability of multi-PRM (mPRM) to predict overall survival. We incorporated 2 physiologically sensitive quantitative imaging maps (ie, rCBV and ADC) into a single mPRM biomarker response metric. This approach retained detailed spatial information on heterogeneity in the tumor response pattern that was critical for improving the predictive sensitivity of the quantitative maps. This study demonstrates that in our patient cohort incorporating multiple metrics into the mPRM voxel-based analysis approach improved the predictive accuracy of the biomarker over the evaluation of a single biomarker.

METHODOLOGY

Patients

Patients with pathologically proven high-grade gliomas were enrolled on a protocol of intratreatment MRI as part of a single-site prospective trial. Informed consent was obtained, and the use of images and medical records was approved by the University of Michigan Institutional Review Board. Only patients with contrast-enhancing tumors of 4 cm³ or greater were included in this study. Fifty-six patients were evaluated before therapy and 3 weeks after the initiation of chemoradiotherapy (Table 1), which consisted of concomitant and adjuvant temozolomide with radiation. Part of this patient cohort had been used previously in published work that investigated the prognostic value of PRM applied to the individual parameters ADC and rCBV and a composite model of PRM applied to these 2 parameters (11, 20, 31).

Radiotherapy was delivered over 6 weeks using standard techniques with a 2.0 to 2.5-cm margin on either the enhancing region on gadolinium (Gd)-enhanced scans or the abnormal signal on T2-weighted scans to 46 to 50 Gy, with the central gross tumor treated to a final median dose of 70 Gy. Chemotherapy was commonly administered in both groups depending upon clinical circumstances (Table 1). No patient received anti-angiogenic therapy during their primary treatment, although some received bevacizumab (Avastin; Genentech) at the time of progression.

MRIs

MRIs were performed 1 week before therapy and 3 weeks after therapy had begun. DW- and dynamic susceptibility contrast (DSC)-MRI and standard MRI (fluid attenuation inversion recovery, T2-weighted, and Gd-enhanced T1-weighted MRI) were conducted on either a 1.5 T Signa (General Electric Medical Systems) or 3 T Achieva (Philips Medical Systems) system. In this study, repeat scans were always acquired on the same MRI scanner as the baseline scan. Radiologic response at 10 weeks was based on changes in tumor volume on T1-weighted contrast-enhanced MRIs and steroid doses and was classified as

Table 1. Clinical Characteristics

Variable	All Patients (n = 56)		Responder (n = 13)		Intermediate (n = 20)		Nonresponder (n = 23)		P Value
	No.	%	No.	%	No.	%	No.	%	
Age (y)	55 (15)		50 (15)		49 (12)		63 (13)		.002
Sex									
Male	24	43	6	46	10	50	8	35	.58
Female	32	57	7	54	10	50	15	65	
Pathology (grade)									
3	10	18	4	31	2	10	4	17	.32
4	46	82	9	69	18	90	19	83	
Karnofsky performance test									
<70	43	77	3	23	2	10	8	35	.14
≥70	13	23	10	77	18	90	15	65	
Location									
Frontal/temporal	35	63	9	69	12	60	14	61	.85
Other	21	37	4	31	8	40	9	39	
Tumor volume (mL)	37 (27)		43 (22)		22 (15)		47 (33)		.01
Radiological response*									
Stable disease/partial response	24	52	10	91	8	53	6	30	.02
Progressive disease	20	44	1	9	6	40	13	65	
Surgery									
Biopsy	21	38	2	15	5	25	14	61	.04
Subtotal	23	41	8	62	9	45	6	26	
Near guided tissue regeneration	12	21	3	23	6	30	3	13	
Radiation therapy (Gy)	68 (9)		70 (8)		68 (9)		66 (9)		.5
Chemotherapy*									
Any	54	96	13	100	20	100	21	91	.16
Temozolomide	52	93	13	100	20	100	19	86	.06
Temozolomide + radiotherapy	31	55	8	62	13	65	10	44	.32

Bold P values indicate statistical significance. The asterisk indicates omitted data for radiological response (10 missing and 2 not available) and chemotherapy (1 missing for "Any"). Likelihood ratio was performed for sex, grade, Karnofsky performance test, location of surgery, and chemotherapy. An ANOVA with a Bonferonni post hoc test was used for age, tumor volume, and radiation therapy dose.

complete response, partial response, stable disease, and progressive disease (6). Steroid doses were recorded before each scan, weekly during radiotherapy, and at each follow-up (32).

DW-MRIs were acquired using a single-shot, spin-echo, diffusion-sensitized, echo planar imaging acquisition sequence. Scans acquired on the 1.5 T system were obtained from 24 6-mm axial-oblique sections using a 22-cm field of view (FOV) and 128 × 128 matrix with *b* factors of 0 and 1000 s/mm² along 3 orthogonal directions (repetition time [TR] = 1000 ms; echo time [TE] = 71–100 ms; number of averages [NS] = 1). Images obtained using the 3 T MRI scanner acquired at least 28 4-mm axial-oblique sections through the brain using a 24-cm FOV and 128 × 128 matrix (TR = 2636 ms; TE = 46 ms; NS = 1 for a *b* value of 0 and NS = 2 for a *b* value of 1000 s/mm²). Parallel imaging (sensitivity encoding factor = 3) was used on the 3 T scanner to reduce spatial distortion. The diffusion-weighted images for the 3 orthogonal directions were used to calculate ADC maps for all patients (20).

To obtain DSC-MRI data, a gradient echo planar imaging pulse sequence was used with the following acquisition parameters: TR = 1.5 to 2 s; TE = 50 to 60 ms; FOV = 22 cm; matrix = 128 × 128; flip angle = 60°; 4–6-mm thickness; 14–20 slices; 0-mm gap. Gd-DTPA (Bayer HealthCare Pharmaceuticals) was injected intravenously with a dose of 0.05 to 0.1 mL/kg as a bolus using a power injector at a rate of 2 mL/s and followed immediately by 15 cc of saline flush at the same rate. A Gd-enhanced T1-weighted image was then acquired. All CBV maps were computed from DSC images as previously described (33). To mitigate the effects from leakage, a preinjection of contrast agent before a second bolus was given during the dynamic T2* imaging (ie, DSC-MRI). In addition, a sufficiently long TR was employed to reduce T1 weighting. To assess differences in tumor blood volume during chemoradiotherapy and among patients, all CBV maps were normalized to CBV values in white matter regions that were contralateral to the tumor to generate rCBV maps. (For simplicity in notation, relative blood volumes for

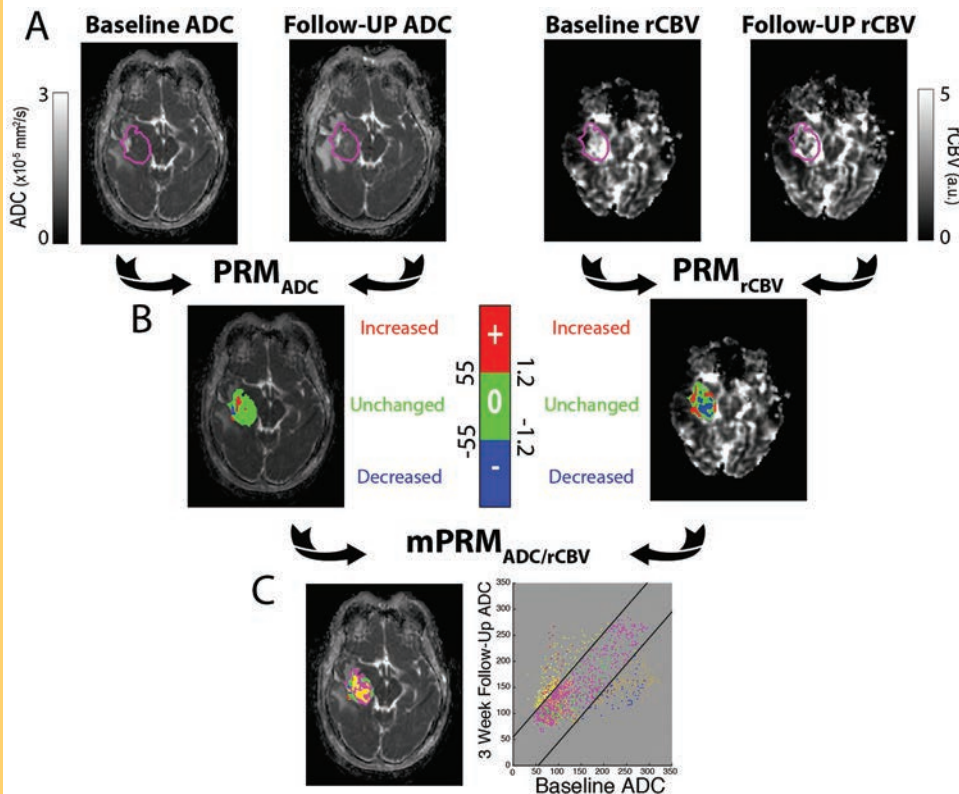


Figure 1. Schematic of the multiparametric PRM technique. (A) Parametric maps of ADC from DW-MRI (left) and rCBV from DSC-MRI (right) acquired before and midway through therapy. (B) The PRM approach was applied to the individually ADC and rCBVs, resulting in 3 classifications each. PRM results are presented as a 3-color overlay that represents regions in which tumor parameter values (ie, ADC or rCBV), based on predetermined thresholds, are unchanged (green voxels), significantly increased (red voxels), or significantly decreased (blue voxels). (C) The individual PRMs are combined, resulting in 9 classifications (2 parameters and 3 classes, resulting in $3^2 = 9$ classes for mPRM). Analogous to mPRM, results are presented as a visual map in which individual voxels are colored by classification as well as presented within a scatter plot. Global measures are presented as relative tumor volumes and calculated as the sum of all voxels in a class normalized to the tumor volume.

both brain and tumor have been denoted by the abbreviation rCBV throughout this article.) White matter regions of interest that were used for normalization were contralateral to the tumor and regions that received an accumulated dose < 30 Gy and avoided regions of partial volume averaging or regions with susceptibility artifacts.

Postprocessing Images

All image data were registered to pretreatment Gd-enhanced T1-weighted images using mutual information as an objective function and the Nelder-Mead simplex as an optimizer (34). Both differently and similarly weighted serial MRIs for the same patient were registered assuming a rigid-body geometric relationship (ie, rotate and translate). After registration, brain tumors were manually contoured by a neuroradiologist over the contrast-enhancing regions of the tumor on Gd-enhanced T1-weighted images.

The PRM of any single parameter (PRM_X , where X denotes any parametric map such as ADC and rCBV) was determined by first calculating the difference between X ($\Delta X = \text{mid-X} - \text{baseline X}$) for each voxel within the tumor before and 3 weeks

after the initiation of treatment. Voxels that yielded a ΔX value greater than a predetermined threshold were designated red (ie, $\Delta \text{rCBV} > 1.2$; $\Delta \text{ADC} > 55$; PRM_{X+}). Blue voxels represented volumes whose parameter value decreased by more than the threshold (ie, $\Delta \text{rCBV} < -1.2$; $\Delta \text{ADC} < -55$; PRM_{X-}), and green voxels represented voxels within the tumor that were unchanged (ie, $|\Delta \text{rCBV}| < 1.2$; $|\Delta \text{ADC}| < 55$; PRM_{X0}). Thresholds were set to 1.2 and 55 for rCBV and ADC, respectively, as determined from previously published work (11, 20, 25). In brief, healthy contralateral brain tissue from registered parameter maps was contoured to generate voxels with paired parameter values at baseline and 3 weeks after treatment was initiated. A linear regression was applied to the data, and the 95% confidence interval (CI) of the fit was used as the threshold for each of the parameters. Thresholds were determined using a subset of patients from this cohort as described in previously published studies (11, 20, 25).

Multiparametric response mapping was applied to ADC and rCBV to generate analytical indices sensitive to changes in both quantitative maps (Figure 1). After image registration as previously described, all serial ADC and rCBV maps shared the same

spatial geometric space, with each voxel having temporal pairs for each biomarker: baseline and midtreatment values of ADC and rCBV. As described previously, PRM applied to a single biomarker results in 3 classifications; when applied to 2 biomarkers voxels it is separated into 9 classifications (3 classifications per biomarker and 2 biomarkers [3²] equal 9 classifications.) The notation used to indicate the mPRM classifications is analogous to PRM for a single biomarker (Figure 1). For example, the volume fraction of tumor characterized as having red on the PRM_{ADC} map (PRM_{ADC}+) and blue on the PRM_{rCBV} map (PRM_{rCBV}-) is named mPRM_{ADC+/rCBV-}.

Statistical Analysis

The 3 classifications for PRM_{ADC} and PRM_{rCBV} and all 9 classifications generated by mPRM_{ADC/rCBV} were assessed for predicting 1-year survival using a receiver operating characteristic (ROC) analysis. The patient population was stratified for each significant metric per PRM model (ie, single and multiparametric) based on optimal cutoffs that maximize sensitivity and specificity in the ROC analysis. Significant single PRM indices were used to generate a 3-tier (ie, composite) PRM model using the same procedure as described in previously published work (31). In brief, PRM_{ADC} and PRM_{rCBV} indices that resulted in a significant prediction of 1-year survival after ROC analysis were combined to stratify the patient population into 3 categorical therapeutic assessments: responders, nonresponders, and intermediate. Patients were designated nonresponders when both PRM indices predicted nonresponding, whereas patients were designated responders when both PRM indices predicted responding. For cases in which PRM indices disagreed, patients were designated intermediate. Because there are 9 metrics gen-

erated by the mPRM analysis, multiple metrics may significantly stratify the patient population based on 1-year survival. In this case, the same 3-tier procedure in combining patient stratification by PRM_{ADC} and PRM_{rCBV} was applied to the significant mPRM indices. Assessing overall survival for all PRM and mPRM models was determined using a Kaplan–Meier analysis with a log-rank test. A multivariate Cox regression with forward entry was used to compare the 3-tier mPRM model to the single-parameter PRM, 3-tier PRM, and individual mPRM models. A secondary analysis was conducted to assess differences in clinical characteristics among outcome groups defined by the 3-tier mPRM model using either a univariate ANOVA with a Bonferroni post hoc test to control for multiple comparisons or a likelihood ratio test. All statistical computations were conducted with a statistical software package (SPSS Software Products), and results were declared statistically significant at the 2-sided 5% comparison-wise significance level ($P < .05$).

RESULTS

Patient Characteristics

A total of 57 patients with high-grade glioma was included in this prospective study (Table 1). The median survival for the population, as determined by the Kaplan–Meier analysis, was 12.8 months (95% CI = 7.2, 18.4), with 50% of the patient population realizing 1-year survival. Patients who died before 1 year had a median survival of 7 months (95% CI = 5.4, 8.6), whereas those whose survival was beyond 1 year had a median survival of 35.1 months (95% CI not available).

mPRM was analyzed by first generating PRM results for individual metrics by spatially aligning temporally paired ADC and rCBV maps to a single geometric frame (Figure 1A) and then

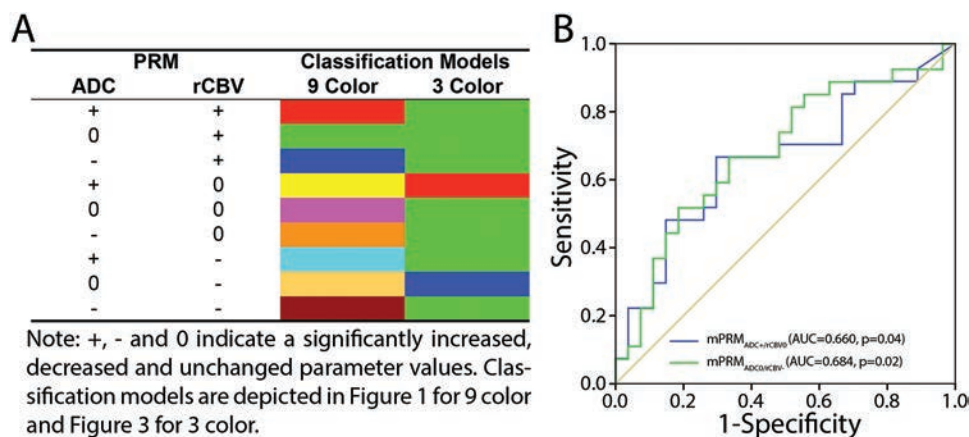


Figure 2. Assessment of predictive mPRM indices. (A) For ease of visualization, the 9 classes generated from the individual PRMs, in which plus (+), minus (-), and 0 represent voxel values that increase, decrease, or remain unchanged, respectively (color code demonstrated in Figure 1), were simplified to a 3-classification scheme. Voxels were color-coded as red for mPRM_{ADC+/rCBV0}, blue for mPRM_{ADC0/rCBV-}, and green for the remaining 7 classifications. (B) Predictive mPRM indices were identified by assessing the potential of the 9 indices to predict 1-year survival using an ROC analysis. Significant ROC stratification was observed in 2 of the 9 classes: mPRM_{ADC+/rCBV0} and mPRM_{ADC0/rCBV-}. These results were used to determine the cutoffs that maximize both sensitivity and specificity for each metric. Cutoffs for response stratification were determined to have relative volumes (RVs) of 2.6% for mPRM_{ADC+/rCBV0} (responders: RV \geq 2.6%; nonresponders: RV $<$ 2.6%) and 4.8% for mPRM_{ADC0/rCBV-} (responders: RV $<$ 4.8%; nonresponders: RV \geq 4.8%).

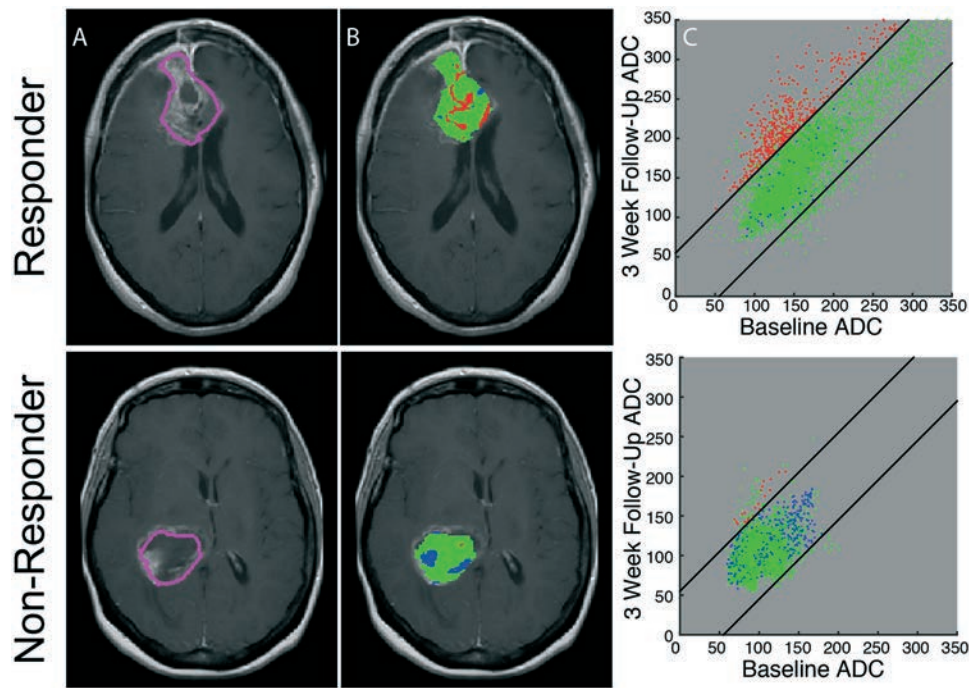


Figure 3. Representative slices from patients identified as responders and nonresponders by mPRM. (A) Presented are T1-weighted post-Gd axial slices with a tumor contour generated from intersecting pretreatment and 3-weeks-of-treatment contours and (B) mPRM overlays with (C) a corresponding mPRM scatter plot for patients identified by mPRM as responder (top) or nonresponder (bottom). The responder was identified as having relative tumor volumes of 10% and 2% for $mPRM_{ADC+/rCBV0}$ and $mPRM_{ADC0/rCBV-}$, respectively. In contrast, the nonresponder had relative tumor volumes of 0% and 14% for $mPRM_{ADC+/rCBV0}$ and $mPRM_{ADC0/rCBV-}$, respectively. Both responders and nonresponders were diagnosed as having stable disease by the Macdonald criteria yet had overall survivals of 64 and 7.1 months, respectively. Scatter plot axes are presented as pretherapy ADC (ie, baseline) for the x-axis and 3-week follow-up ADC for the y-axis. Color coding is based on the 3-color mPRM classification model shown in Figure 2B.

classifying voxels based on previously published thresholds (Figure 1B) (11, 20). Merging the individual PRM data to a single new mPRM resulted in 9 classifications based on changes of both ADC and rCBV at the voxel level (Figures 1C and 2A). Key mPRM classifications were identified using an ROC analysis to assess the potential of each of the 9 classifications for predicting 1-year survival.

In all, 2 of the 9 classifications were identified as predictive of 1-year survival (Figure 2B). The mPRM indices with significantly increasing ADC values and unchanged rCBV ($mPRM_{ADC+/rCBV0}$) values had an area under the curve (AUC) of 0.66 ($P = .04$), whereas mPRM indices with unchanged ADC and significantly decreasing rCBV values ($mPRM_{ADC0/rCBV-}$) had an AUC of 0.684 ($P = .02$). The remaining 7 indices had an AUC near random, with $P > .4$. To simplify the graphical representation on a 3-dimensional image, all voxels classified as $mPRM_{ADC+/rCBV0}$ were color-coded red, those classified as $mPRM_{ADC0/rCBV-}$ were blue, and the remaining voxels were green (Figure 2A). The optimal cutoffs for patient stratification for $mPRM_{ADC+/rCBV0}$ and $mPRM_{ADC0/rCBV-}$ were found to be 2.6% and 4.8% of the tumor volume, respectively. Near-significant results from ROC analyses were observed for PRM_{ADC+} (AUC = 0.651, $P = .057$, cutoff = 4.8%) and PRM_{rCBV-} (AUC = 0.650, $P = .058$, cutoff = 5.5%).

Figure 3 presents representative axial mPRM slices and corresponding scatter plots from 2 patients in which both indices of mPRM identified each patient as a responder or nonresponder 3 weeks into therapy. Figure 2A shows the color coding for the 3-color model. The responder was found to have an $mPRM_{ADC+/rCBV0}$ at 10% of the tumor volume, with 2% of the tumor classified as $mPRM_{ADC0/rCBV-}$. In contrast, the tumor volume from the nonresponder consisted of less than 1% of $mPRM_{ADC+/rCBV0}$, yet 14% consisted of $mPRM_{ADC0/rCBV-}$. Although both patients were diagnosed as having stable disease by the Macdonald criteria, the overall survivals were quite different, with the responder and nonresponder having survival times of 64 and 7 months, respectively.

For an imaging biomarker to be clinically feasible for treatment management, it must be demonstrated as a surrogate marker of overall survival. Figure 4 shows the Kaplan-Meier survival plots for the mPRM indices as well as the combined mPRM model. All analyses produced significant results. As observed in Figure 4A, $mPRM_{ADC+/rCBV0}$ generated a $P = .01$, whereas those identified as nonresponders ($n = 29$) had a median survival of 8.8 months (95% CI = 5.6, 12.0), and responders ($n = 27$) had a median survival of 17.4 months (95% CI not available). Similar results were observed for $mPRM_{ADC0/rCBV-}$, with a $P = .01$ and median survivals for nonresponders ($n = 37$)

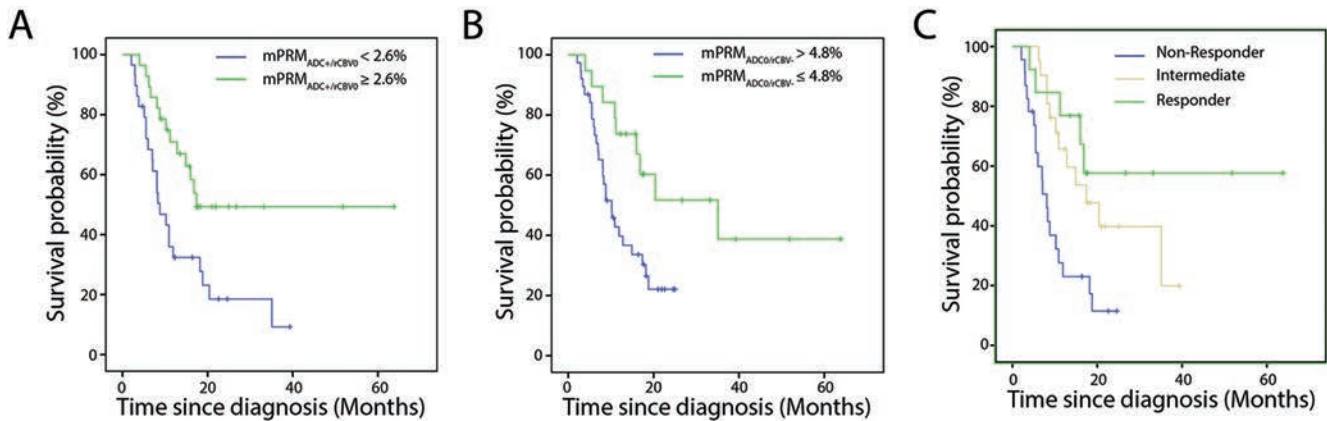


Figure 4. Survival analysis of mPRM biomarkers. Kaplan–Meier survival plots for overall survival are presented for mPRM_{ADC+/rCBV0} (A) and mPRM_{ADC0/rCBV-} (B), where subjects are stratified based on cutoffs determined by ROC analysis (see Figure 2). (C) Overall survival plot for the 3-tier mPRM model. This model separates subjects into 3 groups: responders (mPRM_{ADC+/rCBV0} ≥ 2.6%; mPRM_{ADC0/rCBV-} ≤ 4.8%), nonresponders (mPRM_{ADC+/rCBV0} < 2.6%; mPRM_{ADC0/rCBV-} > 4.8%), and intermediate (remaining combinations).

and responders ($n = 19$) as 10 months (95% CI = 7.5, 13) and 35 months (95% CI = 10, 60), respectively.

Combining the 2 mPRM indices into a 3-tier model improved the potential of the mPRM to predict overall survival (Figure 4C; $P = .002$). Median survivals of the 3 groups were 8.1 months (95% CI = 6.1, 10) for nonresponders, 17 months (95% CI = 8.5, 26) for intermediate, and unattained for responders. A pairwise comparison of the individual pools generated significant results only when comparing nonresponders to either intermediate ($P = .007$) or responders ($P = .005$). No significant differences were observed between intermediate and responders ($P = .2$). When comparing the model to the patient clinical metrics (Table 1), the combined mPRM model was found to significantly vary only for patient age ($P = .002$), initial tumor volume ($P = .01$), radiological response ($P = .02$), and surgical extent ($P = .04$). In short, patients identified as nonresponders were found to be older, had larger initial tumors, underwent biopsies and, as expected, were diagnosed as having progressive disease by radiological response.

Including the intermediate group demonstrated improved performance in the 3-tier model for predicting overall survival beyond what was observed in the single mPRM indices as well as the single-parameter PRM and composite PRM models. Further confirmation was established using a Cox regression analysis with forward entry to assess in a multivariate statistical model which of the single mPRM or PRM schemes provided a better fit to the survival data than what was observed by the 3-tier mPRM model. The Cox regression showed that no further improvement was obtained beyond the inclusion of the 3-tier mPRM in the statistical model ($P = .003$). Controlling for patient age, a known predictor of outcome, did not alter the statistical model results.

DISCUSSION

Because of limited treatment efficacy and radiological phenomena such as pseudoprogression, accurately assessing the thera-

peutic response of gliomas remains a challenge. The updated response assessment criteria for high-grade gliomas reaffirmed the use of anatomical MRI for assessing tumor response to treatments (4). These recommendations suggest evaluating tumor evolution over time based on structural changes observed on both T1-weighted post-Gd and fluid attenuation inversion recovery images 10 to 12 weeks after the start of treatment. Recent studies have shown that morphological changes occur after physiological modifications that may be captured by quantitative MRI techniques (11, 25). The goal of this study was to evaluate a voxel-based approach that generates a response biomarker from 2 physiologically sensitive parameters capable of assessing patient survival after treatment. In this study, mPRM was demonstrated using ADC and rCBV maps and evaluated for how well it predicted overall survival of glioma patients accrued as part of a single-site prospective imaging trial.

Voxel-tracking techniques for assessing responses that demonstrated the value of separating image voxels based on changes in the voxel parametric value from pre- to midtherapy was first introduced in 2005 (25). This approach strongly correlated with a radiological response beyond what was observed using whole-volume tumor summary statistics derived from a histogram analysis (ie, mean change). The voxel-based technique PRM has been shown to be an independent indicator of overall survival as early as 3 weeks after treatment is initiated when applied to either ADC or rCBV and the composite of both (11, 20, 31). As previously reported, PRM_{ADC+}, PRM_{rCBV-}, and the composite PRM model were also found to significantly stratify the patient population ($P = .012$, $.033$, and $.005$, respectively). Although mPRM is analogous to previously published work, the strength of this methodology versus its predecessors is the retention of spatial information that is lost in the composite of PRM_{ADC+} and PRM_{rCBV-} (31). The mPRM technique is a truly voxel-based technique—not a pseudorepresentation of individual PRM analyses of ADC and rCBV. Only 2 of the 9 possible metrics

derived from mPRM, $mPRM_{ADC+/rCBV0}$, and $mPRM_{ADC0/rCBV-}$ were found to be highly predictive of survival after chemoradiotherapy. When combined into a 3-tier model, the potential for predicting overall survival was found to improve over the individual mPRM biomarkers. This highlights the importance of utilizing methods that integrate multiple parameters into a single response map for treatment assessment that can retain spatial information.

Although DW-MRI has become a routine sequence used in most neurological exams, precautions must be taken when acquiring DSC-MRIs to reduce errors in the rCBV measurements. This study implemented all recommendations by Paulson et al. (35) for reducing the impact of the BBB leakage and the T1-weighting effect on CBV measurements. In short, the following protocols were employed: (1) a preinjection of contrast agent before a second bolus (used for the DSC-MRI experiment) to decrease the BBB leakage, (2) a long TR (1.5 to 2 s) to further reduce the T1-weighting effect, and (3) the measurement and use of the arterial input function for each DSC experiment.

The mPRM technique is an extension of the PRM method described in previously published work and as such raises the same issues: changes in the volume of interest size over time and registration. As such, no significant changes of tumors sizes were observed before or 3 weeks after the initiation of treatment in this patient cohort. Moreover, variations observed were below interobserver variability as previously reported for manually tracing brain tumors (36). Problems linked to registration have been extensively discussed in several publications (11, 37, 38). These studies indicate that image-processing approaches can be used effectively to coregister brain MRI data, and registration techniques that apply deformable registration algorithms are also widely available and provide ample flexibility for using mPRM in a wide variety of clinical studies. Because of the limited patient cohort used in this study, the patient character-

istics presented in Table 1 were not controlled for in the Cox regression statistical model when evaluating the different PRM indices. Nevertheless, the mPRM technique can potentially provide a new imaging methodology for assessing treatment response using multiple parametric maps in brain tumor patients. The efficacy of this technique will have to be verified in larger prospective clinical trials, and trials that evaluate newly targeted drugs such as antiangiogenics will be need to be conducted to confirm these findings.

SUMMARY

In this study, we demonstrated in a single-site prospective clinical study an early imaging biomarker to distinguish responding from nonresponding glioma patients to standard-of-care chemoradiotherapy. When evaluated by mPRM and rCBV, ADC metrics, individually known to predict treatment failure, were remarkably found to be spatially delocalized, possibly as a result of different tumor response mechanisms, that is, cell kill as quantified by ADC changes and hypoxia as quantified by a reduction in rCBV values. Merging these parametric biomarkers into a single unique and spatially resolved metric provided additional sensitivity over individual metrics. The mPRM technique shows significant promise as an early and robust imaging biomarker of clinical outcome in patients diagnosed with high-grade gliomas. The application of mPRM could be further extended to evaluate a wide variety of tumor types and other disease processes. Moreover, mPRM could be adapted to include a combination of alternative MRI-based metrics, including vascular permeability, blood flow, and extravascular leakage as well as metrics from other modalities, including, for example, positron emission and computerized tomography. Overall, mPRM is a unique and generalizable imaging biomarker capable of being applied for quantifying dynamic and spatially varying alterations in pathologically relevant disease processes and effects of treatment over time.

ACKNOWLEDGMENTS

C.J.G. and B.L. contributed equally to this work.

This work was supported by National Institutes of Health research grants P01CA085878 and U01CA166104 and Swedish Cancer Foundation grant CAN 2013/321. C.J.G. and B.L. contributed equally to this work.

REFERENCES

- Ostrom QT, Gittleman H, Liao P, Rouse C, Chen Y, Dowling J, Wolinsky Y, Kruchko C, Barnholtz-Sloan J. CBTUS statistical report: primary brain and central nervous system tumors diagnosed in the United States in 2007–2011. *Neuro Oncol*. 2014;16(suppl 4):1–63.
- Stupp R, Hegi ME, Mason WP, van den Bent MJ, Taphoorn MJ, Janzer RC, Ludwin SK, Allgeier A, Fisher B, Belanger K, Hau P, Brandes AA, Gijtenbeek J, Marosi C, Vecht CJ, Mokhtari K, Wesseling P, Villa S, Eisenhauer E, Gorlia T, Weller M, Lacombe D, Cairncross JG, Mirmanoff RO, et al: Effects of radiotherapy with concomitant and adjuvant temozolomide versus radiotherapy alone on survival in glioblastoma in a randomised phase III study: 5-year analysis of the EORTC-NCIC trial. *Lancet Oncol*. 2009;10(5):459–466.
- Brandes D, Stalpers L, Taal W, Sminia P, van den Bent MJ. Clinical features, mechanisms, and management of pseudoprogression in malignant gliomas. *Lancet Oncol*. 2008;9(5):453–461.
- Wen PY, Macdonald DR, Reardon DA, Cloughesy TF, Sorensen AG, Galanis E, De-groot J, Wick W, Gilbert MR, Lassman AB, Tsien C, Mikkelsen T, Wong ET, Chamberlain MC, Stupp R, Lamborn KR, Vogelbaum MA, van den Bent MJ, Chang SM. Updated response assessment criteria for high-grade gliomas: response assessment in neuro-oncology working group. *J Clin Oncol*. 2010;28(11):1963–1972.
- van den Bent MJ, Vogelbaum MA, Wen PY, Macdonald DR, Chang SM. End point assessment in gliomas: novel treatments limit usefulness of classical Macdonald's Criteria. *J Clin Oncol*. 2009;27(18):2905–2908.
- Macdonald DR, Cascino TL, Schold SC, Jr., Cairncross JG. Response criteria for phase II studies of supratentorial malignant glioma. *J Clin Oncol*. 1990;8(7):1277–1280.
- Kickingereder P, Wiestler B, Burth S, Wick A, Nowosielski M, Heiland S, Schlemmer HP, Wick W, Bendszus M, Radbruch A. Relative cerebral blood volume is a potential predictive imaging biomarker of bevacizumab efficacy in recurrent glioblastoma. *Neuro Oncol*. 2015;17(8):1139–1147.
- Schmainda KM, Zhang Z, Prah M, Snyder BS, Gilbert MR, Sorensen AG, Barboriak DP, Boxerman JL. Dynamic susceptibility contrast MRI measures of relative cerebral blood volume as a prognostic marker for overall survival in recurrent glioblastoma: results from the ACRIN 6677/RTOG 0625 multicenter trial. *Neuro Oncol*. 2015;17(8):1148–1156.
- Shiroishi MS, Castellazzi G, Boxerman JL, D'Amore F, Essig M, Nguyen TB, Provenzale JM, Enterline DS, Anzalone N, Dörfler A, Rovira A, Wintermark M, Law M. Principles of T2*-weighted dynamic susceptibility contrast MRI technique in brain tumor imaging. *J Magn Res Imaging*. 2015;41(2):296–313.

10. Law M, Oh S, Babb JS, Wang E, Inglese M, Zagzag D, Knopp EA. Low-grade gliomas: dynamic susceptibility-weighted contrast-enhanced perfusion MR imaging—prediction of patient clinical response. *Radiology*. 2006; 238(2):658–667.
11. Galbán CJ, Chenevert TL, Meyer CR, Tsien C, Lawrence TS, Hamstra DA, Junck L, Sundgren PC, Johnson TD, Ross DJ, Rehemtulla A, Ross BD. The parametric response map is an imaging biomarker for early cancer treatment outcome. *Nat Med*. 2009;15(5):572–576.
12. Batchelor TT, Sorensen AG, di Tomaso E, Zhang W-T, Duda DG, Cohen KS, Kozak KR, Cahill DP, Chen PJ, Zhu M, Ancukiewicz M, Mrugala MM, Plotkin S, Drappatz J, Louis DN, Ivy P, Scadden DT, Benner T, Loeffler JS, Wen PY, Jain RK. AZD2171, a pan-VEGF receptor tyrosine kinase inhibitor, normalizes tumor vasculature and alleviates edema in glioblastoma patients. *Cancer Cell*. 2007; 11(1):83–95.
13. Mangla R, Singh G, Ziegleritz D, Milano MT, Korones DN, Zhong J, Eckholm SE. Changes in relative cerebral blood volume 1 month after radiation-temozolomide therapy can help predict overall survival in patients with glioblastoma. *Radiology*. 2010;256(2):575–584.
14. Hamstra DA, Lee KC, Moffat BA, Chenevert TL, Rehemtulla A, Ross BD. Diffusion magnetic resonance imaging: an imaging treatment response biomarker to chemoradiotherapy in a mouse model of squamous cell cancer of the head and neck. *Transl Oncol*. 2008;1(4):187–194.
15. Chenevert TL, Stegman LD, Taylor JM, Robertson PL, Greenberg HS, Rehemtulla A, Ross BD. Diffusion magnetic resonance imaging: an early surrogate marker of therapeutic efficacy in brain tumors. *J Natl Cancer Inst*. 2000;92(24):2029–2036.
16. Schaefer PW, Grant PE, Gonzalez RG. Diffusion-weighted MR imaging of the brain. *Radiology*. 2000;217(2):331–345.
17. Le Bihan D. The “wet mind”: water and functional neuroimaging. *Phys Med Biol*. 2007;52(7):R57–R90.
18. Le Bihan D. Molecular diffusion nuclear magnetic resonance imaging. *Magn Reson Q*. 1991;7(1):1–30.
19. Anderson AW, Xie J, Pizzonia J, Bronen RA, Spencer DD, Gore JC. Effects of cell volume fraction changes on apparent diffusion in human cells. *Magn Reson Imaging*. 2000;18(6):689–695.
20. Hamstra DA, Galbán CJ, Meyer CR, Johnson TD, Sundgren PC, Tsien C, Lawrence TS, Junck L, Ross DJ, Rehemtulla A, Ross BD, Chenevert TL. Functional diffusion map as an early imaging biomarker for high-grade glioma: correlation with conventional radiologic response and overall survival. *J Clin Oncol*. 2008; 26(20):3387–3394.
21. Liimatainen T, Hakumäki JM, Kauppinen RA, Ala-Korpela M. Monitoring of gliomas in vivo by diffusion MRI and ¹H MRS during gene therapy-induced apoptosis: interrelationships between water diffusion and mobile lipids. *NMR Biomed*. 2009;22(3):272–279.
22. Liu Y, Bai R, Sun H, Liu H, Zhao X, Li Y. Diffusion-weighted imaging in predicting and monitoring the response of uterine cervical cancer to combined chemoradiation. *Clin Radiol*. 2009;64(11):1067–1074.
23. Sadeghi N, D’Haene N, Decaestecker C, Levivier M, Metens T, Maris C, Wikler D, Baleriaux D, Salmon I, Goldman S. Apparent diffusion coefficient and cerebral blood volume in brain gliomas: relation to tumor cell density and tumor microvessel density based on stereotactic biopsies. *AJNR Am J Neuroradiol*. 2008; 29(3):476–482.
24. Lemasson B, Galbán CJ, Boes JL, Li Y, Zhu Y, Heist KA, Johnson TD, Chenevert TL, Galbán S, Rehemtulla A, Ross BD. Diffusion-weighted MRI as a biomarker of tumor radiation treatment response heterogeneity: a comparative study of whole-volume histogram analysis versus voxel-based functional diffusion map analysis. *Transl Oncol*. 2013;6(5):554–561.
25. Moffat BA, Chenevert TL, Lawrence TS, Meyer CR, Johnson TD, Dong Q, Tsien C, Mukherji S, Quint DJ, Gebarski SS, Robertson PL, Junck LR, Rehemtulla A, Ross BD. Functional diffusion map: a noninvasive MRI biomarker for early stratification of clinical brain tumor response. *Proc Natl Acad Sci U S A*. 2005;102(15): 5524–5529.
26. Brisset JC, Hoff BA, Chenevert TL, Jacobson JA, Boes JL, Galbán S, Rehemtulla A, Johnson TD, Pienta KJ, Galbán CJ, Meyer CR, Schakel T, Nicolay K, Alva AS, Hussain M, Ross BD. Integrated multimodal imaging of dynamic bone-tumor alterations associated with metastatic prostate cancer. *PLoS One*. 2015;10(4): e0123877.
27. Tsien C, Galbán CJ, Chenevert TL, Johnson TD, Hamstra DA, Sundgren PC, Junck L, Meyer CR, Rehemtulla A, Lawrence T, Ross BD. Parametric response map as an imaging biomarker to distinguish progression from pseudoprogression in high-grade glioma. *J Clin Oncol*. 2010;28(13):2293–2299.
28. Lausch A, Chen J, Ward AD, Gaede S, Lee TY, Wong E. An augmented parametric response map with consideration of image registration error: towards guidance of locally adaptive radiotherapy. *Phys Med Biol*. 2014;59(22):7039–7058.
29. Hiramatsu R, Kawabata S, Furuse M, Miyatake S, Kuroiwa T. Identification of early and distinct glioblastoma response patterns treated by boron neutron capture therapy not predicted by standard radiographic assessment using functional diffusion map. *Radiat Oncol*. 2013;8(1):192.
30. Ellingson BM, Kim E, Woodworth DC, Marques H, Boxerman JL, Safriel Y, McKinstry RC, Bokstein F, Jain R, Chi TL, Sorensen AG, Gilbert MR, Barboriak DP. Diffusion MRI quality control and functional diffusion map results in ACRIN 6677/RTOG 0625: a multicenter, randomized, phase II trial of bevacizumab and chemotherapy in recurrent glioblastoma. *Int J Oncol*. 2015;46(5):1883–1892.
31. Galbán CJ, Chenevert TL, Meyer CR, Tsien C, Lawrence TS, Hamstra DA, Junck L, Sundgren PC, Johnson TD, Galbán S, Sebolt-Leopold JS, Rehemtulla A, Ross BD. Prospective analysis of parametric response map-derived MRI biomarkers: identification of early and distinct glioma response patterns not predicted by standard radiographic assessment. *Clin Cancer Res*. 2011;17(14):4751–4760.
32. Levin VA, Crafts DC, Norman DM, Hoffer PB, Spire JP, Wilson CB. Criteria for evaluating patients undergoing chemotherapy for malignant brain tumors. *J Neurosurg*. 1977;47(3):329–335.
33. Cao Y, Tsien CI, Nagesh V, Junck L, Ten Haken R, Ross BD, Chenevert TL, Lawrence TS. Survival prediction in high-grade gliomas by MRI perfusion before and during early stage of RT [corrected]. *Int J Radiat Oncol Biol Phys*. 2006;64(3): 876–885.
34. Meyer CR, Boes JL, Kim B, Bland PH, Zasadny KR, Kison PV, Koral K, Frey KA, Wahl RL. Demonstration of accuracy and clinical versatility of mutual information for automatic multimodality image fusion using affine and thin-plate spline warped geometric deformations. *Med Image Anal*. 1997;1(3):195–206.
35. Paulson ES, Schmainda KM. Comparison of dynamic susceptibility-weighted contrast-enhanced MR methods: recommendations for measuring relative cerebral blood volume in brain tumors. *Radiology*. 2008;249(2):601–613.
36. Kaus MR, Warfield SK, Nabavi A, Black PM, Jolesz FA, Kikinis R. Automated segmentation of MR images of brain tumors. *Radiology*. 2001;218(2):586–591.
37. Ellingson BM, Malkin MG, Rand SD, LaViolette PS, Connelly JM, Mueller WM, Schmainda KM. Volumetric analysis of functional diffusion maps is a predictive imaging biomarker for cytotoxic and anti-angiogenic treatments in malignant gliomas. *J Neurooncol*. 2011;102(1):95–103.
38. Ellingson BM, Malkin MG, Rand SD, Connelly JM, Quinsey C, LaViolette PS, et al: Validation of functional diffusion maps (fDMs) as a biomarker for human glioma cellularity. *J Magn Res Imaging*. 2010;31(3):538–548.